Effect of Laser Shock Peening (LSP) on the Phase Evolution, Residual Stress and Hardness of Hastelloy-X Superalloys

Nath, S, Shukla, P, Shen, X & Lawrence, J

ISSN 0898-1507
ESSN 1029-029X

Publisher: Old City Publishing

Effect of Laser Shock Peening on the Phase Evolution, Residual Stress and Hardness of Hastelloy-X Superalloys

SUBHASISA NATH*, PRATIK SHUKLA, XIAOJUN SHEN AND JONATHAN LAWRENCE

Faculty Research Centre for Manufacturing and Materials Engineering, Coventry University, Coventry, CV1 2JH, UK

*Corresponding author: E-mail: sendsubha@gmail.com

Abstract

Efforts have been made to understand the effect of laser shock peening (LSP) on the phase, residual stress and hardness of Hastelloy-X superalloys. A 10 J Nd:YAG laser was used for the LSP operation. Following LSP detailed microstructural and phase analysis along with residual stress and hardness studies were undertaken. A parametric window was first established to explore the relationship between LSP process parameters and the respective surface and bulk properties. The effects of an absorptive layer on the properties of the modified layer were also investigated. Qualitative and quantitative information on dislocation density was obtained using X-ray diffraction (XRD) analysis and correlated with the processing parameters. Residual stress developed following LSP was measured using the XRD technique. An increase in the hardness of the Ni-based superalloys was observed. The residual stress on the surface of the laser shock peened Hastelloy-X superalloy showed a maximum compressive stress of 166 MPa. A detailed microstructure-property relationship was established to understand the mechanism of property enhancement. Further optimization of the LSP process to surface treat the Hastelloy-X superalloys will open up new avenues for the material's applicability, particularly in the aerospace sector.

Keywords: Laser shock peening (LSP); Superalloy; X-ray diffraction (XRD); Hardness; Microstrain; Dislocation density; Residual stress

1 INTRODUCTION

Laser shock peening (LSP) is a process normally used to induce compressive residual stress on the surface of the components that are exposed to a cyclic loading in a normal or corrosive environments [1-4]. The compressive residual stress helps to delay the crack initiation and propagation rate [5, 6]. The LSP treatment, under optimised process parameters, strain hardens the treated zone which in turn improves the tribological properties of the metallic systems [4]. The LSP treatment has also been tried on to ceramic systems [7].

Nickel (Ni) based superalloys are a class of high temperature alloys which shows exceptional strength and resistance in terms of fatigue, creep, and corrosion [8]. Their superior performance at high temperature, allow them to be applicable for engine components in aerospace and automotive industry [8]. However, the demands for increasing the engine efficiency have pushed the engine to its extreme operating conditions. The changing operating conditions have increased the thermal and mechanical loads on the system, thereby, lowering their service life. Thus, strengthening of these materials is of great importance as it increases the efficiency and decreases the repair cost of the engines. The term strengthening means to improve the materials mechanical properties (hardness, fatigue strength, creep strength etc). It is very well known that the strength of materials can be improved by introducing foreign atoms in the matrix as a solid solution, *via* the effect of work hardening, by the formation of precipitates as a result of alloying, and decreasing the grain size of the matrix [9]. On the other hand, fatigue strength in materials can be improved by introducing compressive residual stress (CRS) on the surface of the component [1, 10]. The introduction of CRS on the surface of these components are normally achieved by shot peening (SP) and LSP [1, 11].

The aim of this investigation was to study the effect of LSP on the properties of the Hastelloy-X superalloys and attempts to further understand and verify the strengthening mechanisms as result of LSP surface treatment. In particular, the effect of LSP on the phase

distribution, microstrain, and residual stress evolution was studied using X-ray diffraction (XRD) to understand the contribution of LSP process parameters. Studies were also extended to elucidate the effect of absorptive layer on the development of residual stress on the surface of the superalloys. Finally, dislocation densities were measured to understand the work hardening behaviour of the superalloys followed by a study on the change in the microhardness.

2 EXPERIMENTAL PROCEDURES

2.1 Materials

The LSP was carried out on rectangular Hastelloy-X superalloys samples (30 mm × 10 mm × 10 mm dimension) comprising of composition shown in Table 1. Four superalloy coupons were used for the LSP. The superalloy samples were fully annealed at 1175º for 1 hour to relieve any machining stress. The superalloy samples were then polished using 600 µm grit size SiC papers to clean the surface oxides and residue. The superalloy samples were then ultrasonically cleaned using both acetone and isopropyl alcohol to remove any trapped carbide particles and any other contaminants.

2.2 Laser shock peening

A 10J, pulsed Q-switched Nd:YAG laser system (Litron, LPY10J; Rugby, UK) was used for the experimental study herein. The laser emitted a wavelength of 1064nm. The laser delivered 8ns long pulse with a repetition rate of 10Hz. The laser energy density ranged from 2 to 8 GW/cm^2 by keeping a constant input laser energy of 8J, but altering the laser spot diameter. The beam divergence of the laser was 0.5 mrad with an M^2 value of 1.99. The combined laser beam characteristics and the applied process parameters exhibited a radiance density (laser beam brightness) ranging from 6.44 to 22.651.44 J.Cm^2.Sr^{-1}.µm, determined by

the tried and tested methodology form the previous works [12– 15] as detailed in Table 2. Two samples were laser shock peened (LSPned) without absorptive coatings (LSPwc-1 and LSPwc-2) and the rest two samples were LSPned with absorptive coatings (LSP-3 and LSP-4) as shown in Table 2. Two types of absorptive layers were used during LSP: one is an aluminium tape and the other is a black vinyl tape. All the samples were treated with an overlap of 50%.

According to the principle of LSP, the laser irradiation on the surface of the sample forms an expanding plasma with high pressure shock waves driven into the material. The shock waves with pressure greater than the Hugoniot Elastic Limit (HEL) of the material causes the material to deform plastically. According to Fabbro et al. [16] and Peyre et al. [2], the peak plasma pressure, P, can be expressed as

$$P(GPa) = 0.01\sqrt{\frac{\alpha}{2\alpha+3}}\sqrt{Z\left({}^{g}/_{cm^2s^2}\right)}\sqrt{I_0\left({}^{GW}/_{cm^2}\right)} \qquad (1)$$

where, I_0 is the laser power density, α is the efficiency of the interaction and Z is the reduced shock impedance between the material and the confining medium.

The HEL of any material is related to its dynamic yield strength (σ_Y^{dyn}) as [17]

$$HEL = \frac{1-\vartheta}{1-2\vartheta}\,\sigma_Y^{dyn} \qquad (2)$$

where, υ is the Poisson's ratio of the material.

The laser shock peened (LSPned) parameters were chosen to ensure that the peak plasma pressure exceeds the HEL of the material to plastically deform the material. The LSPned parameters along with peak plasma pressure which was calculated using Equation (1) and HEL which was calculated using Equation (2) are presented in Table 2.

2.3 Material characterisation

2.3.1 Phase analysis

A detailed analysis of the phase evolution was carried out by X-ray diffraction (XRD, D8 Discover; Bruker Corporation) with a scanning speed of 0.05°/s and time per step of 0.1 s using the Cu Kα radiation.

2.3.2 Residual Stress Measurement

Residual stress developed on the surface of the thin films was carefully measured by XRD using a Bragg-Brentano diffractometer (D8 Discover; Bruker Corporation). The X-ray source (Cu K_α radiation) was operated at an accelerating voltage of 40kV and current of 25mA. The XRD was operated at a scanning speed of 0.01°/s and a scanning time of 5s per step. The selected Ψ values were 0 º, 5 º, 10 º, 15 º, 20 º, 25 º, 30 º, 35 º, 40 º, 45 º. For the calculation of residual stress, the (331) peak of γ-Ni phase was considered. The $\sin^2 \Psi$ technique was employed to measure the residual stress values in both the longitudinal and transverse directions. The equation employed to measure residual stress in any given direction, φ, is given by

$$\sigma_\varphi = m \frac{1}{d_0} \left(\frac{E}{1+\vartheta} \right)_{hkl} \qquad (3)$$

where, m is the slope of the d vs $\sin^2\psi$ curve, d_0 is the stress-free lattice spacing ($d_0 \approx d_{\varphi 0}$), E is the Young's modulus and υ is the Poisson's ratio.

2.3.3 Dislocation density measurement

The dislocation density evolution, in the untreated and LSPned samples, was calculated using Wiliamson and Smallman approach [18]. Williamson and Smallman approach assumes the size and strain are related to dislocation density which is true when mechanical milling is used. However, in the present case as LSP was used to plastically deform the material,

microstrain is the only parameter which is affected by plastic deformation and is related to dislocation density. The dislocation density due to strain in the material was calculated from the following relation:

$$\rho = \frac{k\epsilon^2}{b^2} \qquad (4)$$

where, k = 16.1 for F.C.C. crystal, ϵ is the microstrain, b is the burger vector which, for an FCC crystal, is b= (a/2) <110>, where a is the lattice parameter. The lattice parameter in Hastelloy-X superalloy was measured to be 0.255 nm.

2.3.4 Microhardness measurement

The hardness of the untreated and LSP treated samples were measured by Vickers microhardness tester (Struers DURASCAN-70, Denmark) with 50 mN load and a dwelling time of 10 seconds.

3 RESULTS AND DISCUSSION

3.1 X-ray diffraction analysis

XRD phase scans on the untreated Hastelloy-X superalloy (plot 1) and LSPened Hastelloy-X superalloy samples at 7.96 GW/cm^2 with no absorptive tape (plot 2), 2.26 GW/cm^2 with no absorptive tape (plot 3), 2.26 GW/cm^2 with aluminium as an absorptive tape (plot 4), and 2.26 GW/cm^2 with black vinyl tape as an absorptive tape (plot 5) are shown Figure 1. The XRD phase scans confirm the presence of face centred cubic (FCC) Ni as the only phase (matrix) in both untreated and LSPened samples. The LSP treatment on the Hastelloy-X superalloys shows no sign of phase transformation. This is usually expected, and it is indicative that the effects generated herein are similar to cold working. Thus, thermal input as a result of the process was negligible for bringing about such phase transformations which

could otherwise be a possibility with thermos/mechanical effect which the LSP process could also produce.

3.2 Estimation of lattice deformation stress and microstrain by Uniform Stress Deformation Model (USDM)

The Williamson-Hall method for Uniform Deformation Model (UDM) is based on the assumption that the crystals are homogeneous and isotropic in nature (i.e. strain is uniform in all the crystallographic directions) and is represented by the equation [19]:

$$\beta_{hkl} cos\theta_{hkl} = \frac{K\lambda}{D} + 4\,\varepsilon\, sin\theta_{hkl} \qquad (5)$$

where, β is the corrected full width half maximum (FWHM), θ is the diffraction angle, K ($\approx$ 1) is a constant, λ is the X-ray wavelength, D is the crystallite size (or domain size), and ε is the microstrain. The suffix, hkl, refers to a particular crystallographic plane.

It is unrealistic to assume that the crystals are homogeneous and isotropic in nature or the strain is independent of crystallographic directions. So, we have used Uniform Stress Deformation Model (USDM) considering the anisotropic nature of strain. The model assumes a uniform lattice deformation stress (σ). The microstrain (ε) in the Equation (5) can be rewritten as $\varepsilon = \sigma/E_{hkl}$, where E_{hkl} is the Young's modulus in a crystallographic direction perpendicular to the lattice plain (hkl). The crystallographic dependence of the Young's modulus in a cubic crystal is given by

$$\frac{1}{E_{hkl}} = S_{11} - 2\left(S_{11} - S_{12} - \frac{1}{2}S_{44}\right)\left(\frac{(h^2k^2 + k^2l^2 + k^2l^2)}{(h^2 + k^2 + l^2)^2}\right)$$

where, S_{11}, S_{12}, and S_{44} are the elastic compliance which, for a Ni alloy, are 7.67 TPa^{-1}, 2.93 TPa^{-1}, and 8.23 TPa^{-1}, respectively [20]. The values of Young's modulus corresponding to different crystallographic planes are presented in Table 3-7.

Re-writing Equation (5), whilst considering anisotropy in microstrain or lattice deformation stress as

$$\beta_{hkl} cos\theta_{hkl} = \frac{K\lambda}{D} + 4\left(\frac{\sigma}{E_{hkl}}\right) sin\theta_{hkl} \quad (6)$$

Figure 2 shows the plots between $\beta_{hkl}\cos\theta$ and $4\sin\theta/E_{hkl}$ for (a) an untreated Hastelloy-X; (b) LSPwc-1; (c) LSPwc-2; (d) LSP-3; and (e) LSP-4. From the slope and intercept of the plot between $\beta_{hkl}\cos\theta$ and $4\sin\theta/E_{hkl}$, the lattice deformation stress, σ, and the crystallite size, D, have been measured, respectively. The measured values of microstrain and lattice deformation stress in an untreated and LSPned Hastelloy-X samples are presented in Table 3-7.

The lattice deformation stress in an untreated Hastelloy-X sample is 49 MPa as shown in Table 3. The lattice deformation stress in LSPwc-1 is 290 MPa which is maximum among the other studied systems (*cf*. Table 4-7). A high value of lattice deformation stress in a sample implies that the sample has undergone a significant amount of plastic deformation due to LSP which is attributed to the use of higher power density in LSPwc-1 sample. The lattice deformation stress in LSPwc-2 was found to be 283 MPa and is well above the LSP-3 and LSP-4 systems. This was due to a higher portion of the laser energy transferred to the sample rather than creating a shock wave with high pressure since the absence of an absorptive layer. The lattice deformation stresses in LSP-3 and LSP-4 systems were measured to be 257 MPa and 198 MPa, respectively. Comparing LSP-3 and LSP-4, it can be concluded that the aluminium tape as an absorptive layer was effective in creating maximum lattice deformation stress than the black vinyl tape.

3.3 Dislocation density

3.3.1 Qualitative analysis

Intensity of plastic deformation in the material due to LSP is directly related to the microstrain developed in the crystal lattice. An increase in the microstrain (peak broadening) implies an increase in the dislocation density. LSP of Hastelloy-X superalloys shows that the microstrain (or the plastic deformation) developed on the surface of the Hastelloy-X samples is dependent on the peak power density of the laser as shown in Table 8. With a peak power density of 7.96 GW/cm^2, the microstrain in the crystal lattice shows a maximum value of 1.46 × 10^{-3}. Lowest microstrain is measured in the LSP-4 sample where the peak power density of 2.26 GW/cm^2 was used with a black vinyl tape as an absorptive layer. The increase in microstrain in LSPwc-1 is attributed to increase in the shock wave pressure resulting from higher power density according to Equation (1).

3.3.2 Quantitative analysis

Another way to quantify plastic deformation is to measure the dislocation density. Dislocations are the result of plastic deformation in the materials. A higher dislocation density, not only, implies a hardened surface, but also, forms a nanocrystalline structure on the surface which increases its strength. In the present study, dislocation density in the untreated and LSPned superalloys were measured using Wiliamson and Smallman approach [18]. This approach considers crystallite size and microstrain as the factors responsible for dislocations density. However, an increase in the dislocation density increases the full width half maximum (FWHM) of the XRD peak which is directly related to the microstrain in the crystal lattice. Table 8 presents the dislocation densities in an untreated and LSPned Hastelloy-X superalloys. The LSP of Hastelloy-X superalloys show an increase in the dislocation density as compared to that of the untreated superalloy. This observation indicates that the chosen laser processing parameters are acceptable and corroborates well with the

theory of LSP (Equation (1)). Surprisingly, the dislocation density in LSPwc-1 sample is the highest amongst the other LSPned samples. The sample LSPned with a power density of 7.96 GW/cm^2 shows highest dislocation density. The use of an absorptive layer in LSP decreases the dislocation density as shown in Table 8. This is not usual as it is believed that the use of absorptive coatings increases the shock wave pressure in the material. The observation can be related to the fact that both thermal and mechanical effects were present in LSPwc-1 and LSPwc-2. The decrease in dislocation densities in LSP-3 and LSP-4 as compared to LSPwc-1 and LSPwc-2 is believed due to the partial loss in the incident laser energy due to melting and evaporation of absorptive coatings in LSP-3 and LSP-4 samples. Comparing LSP-3 and LSP-4, it can be concluded that the aluminium based absorptive coating increases the dislocation density in the material. This is possibly due to increased shock pressure in the Hastelloy-X superalloys with aluminium as an absorptive layer as compared to that of black vinyl tape.

3.4 Residual stress analysis

Residual stress developed on the surface of the untreated and LSPned samples are presented in Table 9. As shown in Table 9, the residual stress in an untreated Hastelloy-X sample is tensile in nature with 23 MPa and 25 MPa in longitudinal and transverse directions, respectively. Lower values of residual stress measured on the surface of an untreated Hastelloy-X are due to the full annealing operation performed on the samples. The residual stresses developed on the surface of LSPned Hastelloy-X samples without absorptive coatings show tensile stresses in both longitudinal and transverse directions despite being the obvious benefits which the process introduces in general. The reason behind the developed tensile stresses on the surfaces of LSPwc-1 and LSPwc-2 is due to the dominant thermal effect (melting and evaporation) instead of mechanical effect. Normally, an absorptive coating is used to avoid thermal effects and ensure a pure mechanical effect develops on the surface of the samples. However, in the case of LSPwc-1 and LSPwc-2, most of the energy

was used to melt and evaporate a thin layer of the sample rather than creating shock pressure which is rather needed for inducing compressive residual stress on the surface. Such phenomena was observed by Masse and Barreau [21] and Gill et al. [22]. On the hand, the residual stresses developed on the surface of the LSP-3 and LSP-4 shows compressive in nature. The measured compressive nature of the stresses in the LSP-3 and LSP-4 samples are due to the use of the absorptive coatings which prevented the samples surface to get melted and generate the necessary shock pressure in the material in order to induce compressive residual stresses. The developed shock pressure on the surface of the samples are responsible for the formation of compressive residual stresses on the surface of LSP-3 and LSP-4.

It is interesting to note that the surface treated with aluminium tape shows the maximum residual compressive stress than the surface treated with black vinyl tape as shown in Table 9. The reason behind such a difference in generation of stresses on the surface of the Hastelloy-X samples is related to the developed peak pressure in aluminium tape as compared to black vinyl tape.

3.5 Microhardness distribution

The improvement in microhardness is related to the strain hardening phenomena due to LSP. Figure 3 shows the microhardness distribution in the LSPned samples LSP-3 and LSP-4. The samples LSP-3 and LSP-4 were chosen for the microhardness measurement as they showed compressive residual stress on the surface. From Figure 3, it is evident that the microhardness on the surface is higher than the interior. The tail end of the microhardness curve presents the microhardness value of an untreated superalloy (~260 VHN). The increased microhardness on the surface of the LSP treated sample is related to the strain hardening of the surface layer due to increased dislocation density (*cf*. Table 8). The gradual decrease in the microhardness values of the LSP-3 and LSP-4 samples with depth is related to the decrease in the dislocation

density with depth. The material, normally, experiences a maximum shock pressure due to LSP on the surface which gradually decreases towards the depth. As the amount of plastic deformation is dependent on the shock wave pressure, the plastic deformation decreases with depth. The LSPned superalloy with aluminium as an absorptive layer (LSP-3) shows maximum improvement in hardness with ~380 VHN as compared to ~360 VHN in the LSP-4. The improvement in microhardness in LSP-3 is related to the increased dislocation density and higher compressive residual stress.

4 CONCLUSIONS

A comprehensive investigation of LSP surface treatment of Hastelloy-X superalloys was undertaken using a 10J Nd:YAG laser to understand the evolution of structure and properties as well as to understand the strengthening mechanisms. The LSP surface treatment was carried out on the bare Hastelloy-X superalloys as well as on the superalloys coated with aluminium and black vinyl tape as absorptive layers. The process parameters were chosen to ensure plastic deformation in the material based on the classical theory of shock wave (2.26 GW/cm^2 and 7.96 GW/cm^2).

From the study, the following conclusions may be drawn:

(i) The LSP treatment showed no sign of phase transformation ensuring that the sample's surface structure was stable after LSP treatment.

(ii) The lattice deformation stress was found to increase with increase in the peak power density. A higher lattice deformation stress of 290 MPa was obtained for Hastelloy-X samples LSP treated without an absorptive layer.

(iii) A larger microstrain of 1.52×10^{-3} was developed on the surface of the Hastelloy-X sample with LSP treated at highest power density and without an absorptive tape. Use of aluminium as an absorptive layer during LSP showed an increase in the

microstrain (1.29×10^{-3}) in the crystal lattice of Hastelloy-X superalloy in comparison to the black vinyl tape (0.998×10^{-3}).

(iv) Tensile stresses were developed on the Hastelloy-X superalloys when they were subjected to LSP without any absorptive layer. On the other hand, compressive residual stresses of 48 - 166 MPa were developed on the surface of Hastelloy-X superalloys when they were LSPned with aforementioned absorptive layers. Maximum compressive residual stress of 166 MPa was observed on the Hastelloy-X superalloy when LSPned with aluminium absorptive layer.

(v) Dislocation densities were found to be more when the samples were LSPned without an absorptive layers implying higher plastic deformation in the sample. High laser power density was also able to increase the dislocation density in the Hastelloy-X samples.

(vi) Strain hardening was more on the samples treated with aluminium absorptive layer compared to black vinyl tape. A maximum hardness of ~380 VHN was found with aluminium absorptive layer compared to ~360 VHN for black vinyl tape.

5 Acknowledgments

The authors of this paper would like to thank EPSRC funded laser loan pool scheme for granting a state-of-the-art shock peening laser system (Grant no: 13250017 (NSL4)) and all those whom have been associated with the projects directly and indirectly.

NOMENCLATURE

a	Lattice parameter (nm)
b	Burger vector (nm)
d_0	Stress-free lattice spacing (nm)
D	Crystallite size (nm)
E	Young's modulus (GPa)
HEL	Hugoniot elastic limit (GPa)
I_0	Laser power density (GW/cm^2)
P	Shock wave pressure (GPa)
S	Elastic compliance factor (TPa^{-1})
Z	Reduced shock impedance between the material and the confining medium (g/cm^2s^2)

Greek symbols

α	Efficiency of the interaction between the material and the confining medium
β	Full width half maximum, FWHM (radian)
ρ	Dislocation density (m^{-2})
d_0	Stress free interplanar lattice spacing (nm)
ε	Microstrain in a crystal lattice
σ_Y^{dyn}	Dynamic yield strength (GPa)
σ	Lattice deformation stress (MPa)
σ_φ	Residual stress at an angle, φ (MPa)
φ	Angle between a fixed direction in the plane of the sample and the projection in that plane of the normal of the diffracting plane
Ψ	Angle between the normal of the sample and the normal of the diffracting plane (bisecting the incident and diffracted beams)
θ	Diffraction angle (^{o})
λ	X-ray wavelength (A^o)

REFERENCES

[1] Peyre P. and Fabbro R. Laser shock processing: A review of the physics and applications. *Optical and Quantum Electronics* **27**(12) (1995), 1213-1229.

[2] Peyre P., Fabbro R., Merrien P. and Lieurade H.P. Laser shock processing of aluminium alloys. Application to high cycle fatigue behaviour. *Materials Science and Engineering A* **210** (1-2) (1996), 102-113.

[3] Lu J.Z., Qi H., Luo K.Y., Luo M. and Cheng X.N. Corrosion behaviour of AISI 304 stainless steel subjected to massive laser shock peening impacts with different pulse energies. *Corrosion Science* **80** (2014), 53–59.

[4] Lim H., Kim P., Jeong H. and Jeong S. Enhancement of abrasion and corrosion resistance of duplex stainless steel by laser shock peening. *Journal of Materials Processing Technology* **212** (6) (2012), 1347– 1354.

[5] Montross C.S., Wei T., Ye L., Clark G. and Mai Y.W. Laser shock processing and its effects on microstructure and properties of metal alloys: a review. *International Journal of Fatigue* **24** (10) (2002), 1021–1036.

[6] Rubio-González C., Felix-Martinez C., Gomez-Rosas G., Ocana J.L., Morales M. and Porro J.A. Effect of laser shock processing on fatigue crack growth of duplex stainless steel. *Materials Science and Engineering A* **528** (3) (2011), 914–919.

[7] Shukla P., Nath S., Wang G., Shen X. and, Lawrence J. Surface property modifications of silicon carbide ceramic following laser shock peening. *Journal of the European Ceramic Society*. **37** (9) (2017), 3027-3038.

[8] Reed R.C. *The Superalloys: Fundamentals and Applications*. New York: Cambridge University Press. 2006.

[9] Callister W.D.Jr, Rethwisch D.G. *Materials Science and Engineering*. New Jersey: John Wiley & Sons. 2014.

[10] James M.N., Hughes D.J., Chen Z., Lombard H., Hattingh D.G., Asquith D., Yates J.R. and Webster P.J. Residual stresses and fatigue performance. *Engineering Failure Analysis* **14** (2) (2007), 384–395.

[11] Raghavan R., Ayer R., Jin H.W., Marzinsky C.N. and Ramamurty U. Effect of shot peening on the fatigue life of a Zr-based bulk metallic glass. *Scripta Materialia* **59** (2) (2008), 167–170.

[12] Shukla P.P. and Lawrence, J. The influence of brightness whilst laser surface processing of a silicon nitride engineering ceramic. *Optics and Lasers in Engineering* **50** (2012), 1746-17512.

[13] Shukla, P.P. and Lawrence, J. Role of laser beam radiance in different ceramic processing: A two wavelength comparison. *Optics and Laser Technology* **54** (2013), 380 – 388.

[14] Shukla, P., Lawrence J. and Zhang, Yu. Understanding laser-beam brightness: a review on a new prospective in materials processing. *Optics and Lasers in Engineering* **75** (2015), 40 – 51.

[15] Shukla, P.P. and Lawrence, J. Identification of optical parameters for determination of radiance. *Journal of Optics* **44** (1) (2015), 12-19.

[16] Fabbro R., Fournier J., Ballard P., Devaux D. and Virmont J. Physical study of laser-produced plasma in confined geometry. *Journal of Applied Physics* **68** (2) (1990), 775–784.

[17] Johnson J.N. and Rohde R.W. Dynamic deformation twining in shock-loaded iron. *Journal of Applied Physics*. **42** (11) (1971), 4171–4182.

[18] Williamson G.K. and Smallman R.E. Dislocation densities in some annealed and cold worked metals from measurements on the X-Ray Debye-Scherrer spectrum. *Philosophical Magazine*. **1** (1) (1956), 34-46.

[19] Suryanarayana C. and Norton M.G. *X-Ray Diffraction: a practical approach*. New York: Springer. 1998.

[20] Gale W.F. and Totemeier T.C. (Ed.). *Smithells Metals Reference Book*. The Netherlands: Elsevier. 2004.

[21] Masse J.E. and Barreau G. Laser generation of stress waves in metal. *Surface and Coatings Technology*. **70** (2-3) (1995), 231-234.

[22] Gill A.S., Telang, A. and Vasudevan V.K. Characteristics of surface layers formed on inconel 718 by laser shock peening with and without a protective coating. *Journal of Materials Processing Technology*. **225** (2015), 463–472.

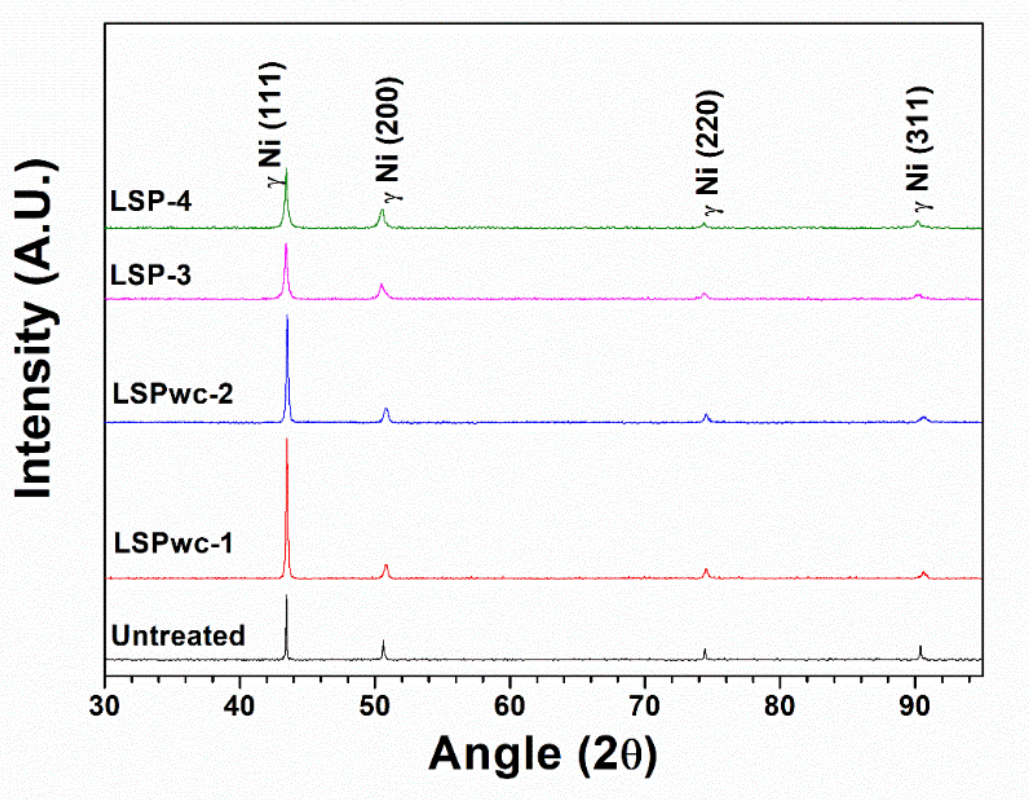

FIGURE 1 X-ray diffraction scans of untreated and LSPned surface under different processing conditions.

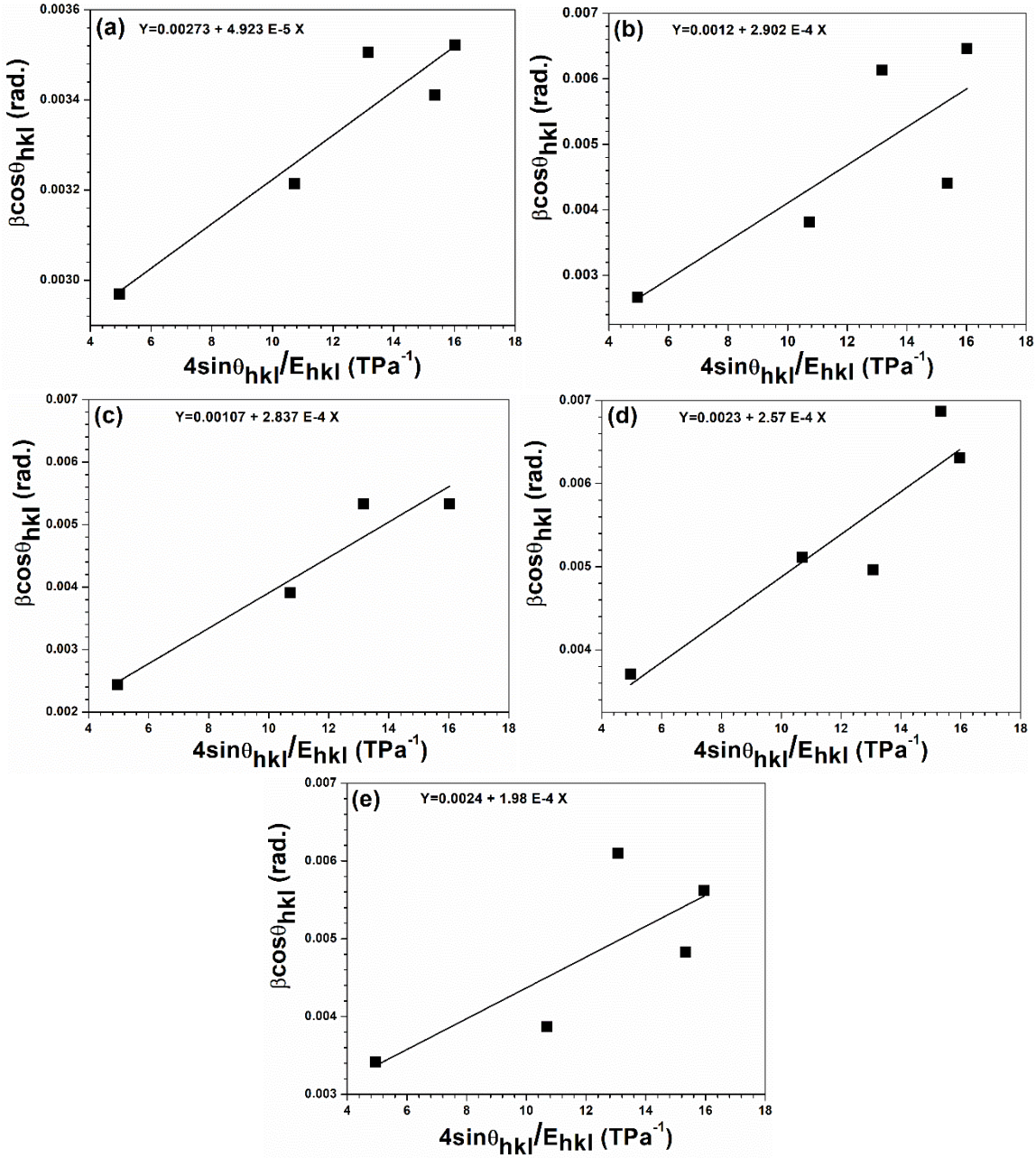

FIGURE 2 Williamson-Hall plots for (a) an untreated Hastelloy-X sample, (b) LSPwc-1, (c) LSPwc-2, (d) LSP-3, and (e) LSP-4.

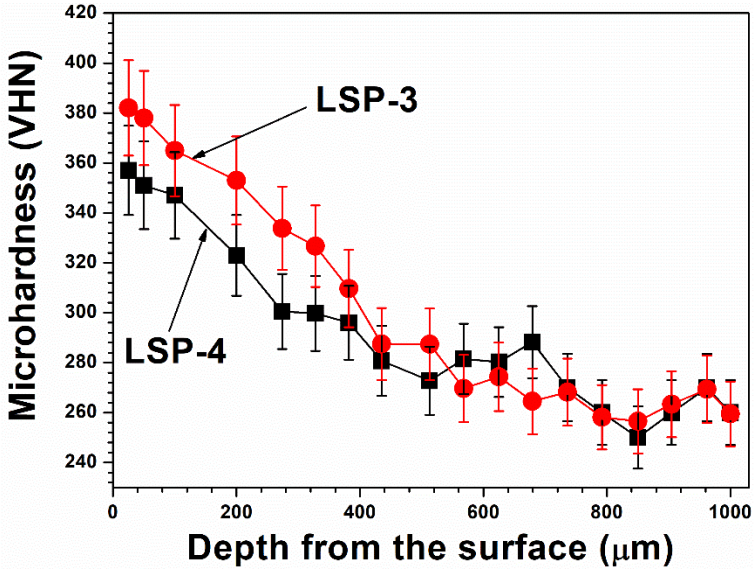

FIGURE 3 Microhardness distribution with depth in LSP-3 (plot 1) and LSP-4 (plot 2) Hastelloy-X superalloy sample.

TABLE 1 Composition of Hastelloy-X used for LSP.

Composition (wt%)						
Ni	Cr	Fe	C	Mo	Si	W
Bal.	20	19.8	7.6	7	0.3	0.5

TABLE 2 Laser shock peening parameters used in the present study.

Sample	Energy (J)	Spot size (mm)	Peak power density (GW/cm^2)	Radiance density (Brightness, $J.cm^2.Sr^{-1}.\mu m$)	Absorptive layer	Overlap (%)	Peak pressure (GPa)	HEL (GPa)
LSPwc-1	8	4	7.96	22.65	No layer	50	2.88	1.11
LSPwc-2	8	7.5	2.26	6.44	No layer	50	1.53	1.11
LSP-3	8	7.5	2.26	6.44	Aluminium tape	50	1.53	1.11
LSP-4	8	7.5	2.26	6.44	Black vinyl tape	50	1.53	1.11

TABLE 3 Young's modulus, microstrain, and lattice deformation stress in an untreated Hastelloy-X sample.

Plane (hkl)	Young's modulus (MPa)	Microstrain (ϵ_{hkl})	Lattice deformation stress, σ (MPa)
111	229	0.00017	49
200	130	0.00038	
220	226	0.00022	
311	178	0.00028	
331	243	0.00020	

TABLE 4 Young's modulus, microstrain, and lattice deformation stress in LSPwc-1.

Plane (hkl)	Young's modulus (MPa)	Microstrain (ϵ_{hkl})	Lattice deformation stress, σ (MPa)
111	229	0.00097	290
200	130	0.00222	
220	226	0.00128	
311	178	0.00163	
331	243	0.00119	

TABLE 5 Young's modulus, microstrain, and lattice deformation stress in LSPwc-2.

Plane (hkl)	Young's modulus (MPa)	Microstrain (ϵ_{hkl})	Lattice deformation stress, σ (MPa)
111	229	0.00095	283
200	130	0.00217	
220	226	0.00125	
311	178	0.00159	
331	243	0.00116	

TABLE 6 Young's modulus, microstrain, and lattice deformation stress in LSP-3.

Plane (hkl)	Young's modulus (MPa)	Microstrain (ϵ_{hkl})	Lattice deformation stress, σ (MPa)
111	229	0.00086	257
200	130	0.00197	
220	226	0.00114	
311	178	0.00145	
331	243	0.00106	

TABLE 7 Young's modulus, microstrain, and lattice deformation stress in LSP-4.

Plane (hkl)	Young's modulus (MPa)	Microstrain (ϵ_{hkl})	Lattice deformation stress, σ (MPa)
111	229	0.00066	198
200	130	0.00152	
220	226	0.00088	
311	178	0.00112	
331	243	0.00081	

TABLE 8 Average microstrain and dislocation density in untreated and LSPned Hastelloy-X superalloy samples.

Sample	Average microstrain, $\epsilon \times 10^{-3}$	Dislocation density, $\rho \times 10^{14}$ (m^{-2})
Untreated	0.25	0.16
LSPwc-1	1.46	5.28
LSPwc-2	1.43	5.06
LSP-3	1.29	4.12
LSP-4	0.998	2.47

TABLE 9 Residual stress developed in the untreated and LSPned Hastelloy-X superalloy samples.

Sample	Residual stress (MPa)	
	σ (Longitudinal)	σ (Transverse)
Untreated	23 ± 13	25 ± 11
LSPwc-1	149 ± 28	135 ± 25
LSPwc-2	121 ± 11	124 ± 22
LSP-3	-166 ± 15	-132 ± 23
LSP-4	-117 ± 21	-48 ± 18